Materials Transactions, Vol. 43, No. 4 (2002) pp. 681 to 687

Structure and Transport Properties of $(Bi_{1-x}Sb_x)_2Te_3$ Thermoelectric Materials Prepared by Mechanical Alloying and Pulse Discharge Sintering

Liu Xue-Dong * and Yong-Ho Park

National Institute of Advanced Industrial Science and Technology (AIST Tohoku), Sendai 983-8551, Japan

Mechanical alloying followed by pulse discharge sintering (MA-PDS) has been employed to develop the bulk $(Bi_{1-x}Sb_x)_2Te_3$ thermoelectric materials with various Sb alloying contents. Substitutional solid solutions of $(Bi_{1-x}Sb_x)_2Te_3$ are formed in the whole Sb content range by MA-PDS process. The sintered compacts are dense and have refined microstructures. Systematic investigations on the electrical, thermal and thermoelectric properties reveal that the transport properties of the obtained $(Bi_{1-x}Sb_x)_2Te_3$ samples are quite sensitive to the Sb alloying content. At room temperature, the samples with $x < 0.57$ exhibit n-type semi-conduction. However, at $x > 0.57$, the samples become p-type. The pure constituents of Bi_2Te_3 and Sb_2Te_3 as well as the Sb-poor, n-type samples exhibit the room-temperature figure of merit of the order of $1.0 \times 10^{-3}\,K^{-1}$. High values of figure of merit have been obtained in the Sb-rich, p-type samples. The maximum value of $3.35 \times 10^{-3}\,K^{-1}$ is attained at $x = 0.80$, which corresponds to the carrier concentration and Hall mobility of $1.95 \times 10^{19}\,cm^{-3}$ and $207\,cm^2/Vs$, respectively.

(Received November 27, 2001; Accepted February 18, 2002)

Keywords: *mechanical alloying, pulse discharge sintering, $(Bi, Sb)_2Te_3$, transport property*

1. Introduction

Bi_2Te_3, Sb_2Te_3 and their solid solutions $(Bi, Sb)_2Te_3$ are of great interest for near-room-temperature applications in thermoelectric (TE) cooling devices.[1–3] As a measure of the performance of a thermoelectric device, the figure of merit of the constituent TE material (Z) is defined by $Z = S^2\sigma/\kappa$, where S, σ and κ are respectively the Seebeck coefficient, electrical conductivity and thermal conductivity. The bulk Bi_2Te_3-based thermoelectric materials are now available by several existing techniques such as unidirectional casting and powder metallurgy.[4–7]

Powder processing, say hot/cold pressing, is an effective technique for fabricating the bulk TE materials. This approach is superior to the conventional unidirectional solidification for single-crystal growth in some aspects. For example, it is very simple in processing, and the refined microstructure produced by powder metallurgy eliminates the possibility of catastrophic failure of the product due to cleavage and thus increases the mechanical strength. Two ways are now available for producing powders by either mechanical alloying of the elemental powders or mechanical grinding of the pre-melted ingot. Some early studies[4–6] indicated that solid solutions of $(Bi_{1-x}Sb_x)_2Te_3$ over the entire compositional range of Sb are available by powder metallurgy. Transport property measurements demonstrated that the hot-pressed p-type $(Bi_{1-x}Sb_x)_2Te_3$ polycrystals showed room-temperature figure of merit values that were close to or greater than $3.0 \times 10^{-3}\,K^{-1}$ at the Sb alloying level of $0.70 \leq x \leq 0.80$. On the other hand, unlike single crystals, the sintered $(Bi_{1-x}Sb_x)_2Te_3$ polycrystals will not retain a single sign of charge carriers as x changes. For example, a p-n transition was reported in the pressed $(Bi_{1-x}Sb_x)_2Te_3$ alloys at $x = 0.67$.[4] Below $x = 0.67$, the alloys are n-type, above it the alloys become p-type.

A new processing technique, mechanical alloying followed by pulse discharge sintering (MA-PDS), has been developed in our laboratory to fabricate the bulk Bi_2Te_3-based thermoelectric materials.[7] In this processing, mechanical alloying (MA) allows the formation of extremely fine $(Bi, Sb)_2Te_3$ solid solution crystallites from the elemental powders of Bi, Sb and Te through a sequence of collision events inside a ball mill. The mechanically alloyed powders are subsequently compacted into bulk by pulse discharge sintering (PDS) for further microstructure and transport property characterizations. In comparison to the conventional hot-pressing process, the very short time and the low temperature exposure of MA powders achieved by PDS offers the best means to retain fine grain size in compacts. Therefore, the combination of MA and PDS processes may result in very fine microstructures of the final product. In a previous study, we have successfully synthesized the bulk $(Bi_{0.25}Sb_{0.75})_2Te_3$ alloys with various contents of Ag and BN by MA-PDS process.[7] As a continuous study, in this work the bulk $(Bi_{1-x}Sb_x)_2Te_3$ alloys with various x values were made by means of this new technique. A systematic investigation on the microstructure and the transport properties of the bulk samples was conducted as a function of the Sb content. The purposes are to examine how the Sb content affects the transport behavior of the compact, and, meanwhile, to explore the possibility of optimizing the room-temperature figure of merit of the Bi_2Te_3 alloy by Sb alloying.

2. Experimental Procedures

5N elemental powders of bismuth (−80 mesh), tellurium (−100 mesh) and antimony (−100 mesh) were selected as starting materials for mechanical alloying. MA was carried out in a vibratory ball mill under the fixed vibration frequency of 25 Hz. The stainless steel vial with ZrO_2 lining and ZrO_2 balls of 15.5 mm diameter were utilized. The elemental powders in the desired composition were pre-mixed and loaded into the vial at the ball-to-powder mass ratio of 75:1. The milling was conducted in argon atmosphere for 200 h without interruption. All the powder handling was done in an

*Corresponding author: Email: liu-dong@aist.go.jp

argon-filled glove box, in which the oxygen level is kept below 5 ppm, to prevent the powders from oxidation. Typically, about 25 g of the alloyed powders were obtained after each run.

The mechanically alloyed powders were sieved and the powders under 28 μm were used for the subsequent pulse discharge sintering (PDS). PDS was performed in a DR.SINTER SPS-1020 system in vacuum (10^{-3} Pa). Graphite molds and punches were used with sprayed BN particle coating to reduce friction during compact ejection. The temperature and pressure programs were shown in Fig. 1. The initial pressure applied was 16 MPa. At 473 K, the pressure was raised to 50 MPa. And the load was kept at 50 MPa until the whole sintering process finished. During sintering, a direct electric current with imposed pulse waves, the intensity of which is proportional to the temperature, was applied. The sintering temperature was measured using the thermocouple inserted into the mold. The resultant compact is a column of 5–10 mm height and 20 mm diameter.

X-ray diffraction (XRD) of the as-milled powders and the as-sintered compacts was carried out in a Philips X'Pert-MPD system (Cu Kα) over a 2θ span of 20° to 80°. Scanning electron microscope (SEM) observations on the fracture surfaces of the compacts were made along the pressing direction on a Philips XL-30S system. SEM was operated at an accelerating voltage of 10 kV.

Samples in the forms of disk and pillar were cut from the columnar compacts by electro-discharge machine (EDM) for Hall effect, thermal diffusivity and Seebeck coefficient measurements. All the measurements were made with the heat/current flow perpendicular to the pressing direction. Electrical resistivity (ρ), Hall coefficient (R_H), carrier concentration (n) and Hall mobility (μ_H) were determined from 80 K to 380 K on a ResiTest 8300 DC Hall Measurement apparatus. We used liquid nitrogen to cool the samples. A constant magnetic field of 0.86 T was applied during the Hall coefficient measurement. The carrier concentration (n) was calculated from the Hall coefficient, assuming a single carrier model and a Hall scattering factor of unity, by $n = 1/(R_H e)$, e is the electronic charge. The Hall mobility (μ_H) was calculated from the Hall coefficient (R_H) and the electrical resistivity (ρ) values by $\mu_H = R_H/\rho$. The errors were estimated to be ±1% and ±2% for the resistivity and the Hall coefficient data, respectively. Density of the compact was determined by the Archimedes method. Specific heat capacity (c_p) was determined on a differential scanning calorimeter (DSC, Seiko EXSTAR DSC6200). We use pure sapphire as the standard sample. The thermal diffusivity (κ_d) was determined on a Laser Flash TC-7000 Thermal Constant Analyzer in vacuum. The thermal conductivity (κ) was calculated from the experimental density (d), heat capacity (c_p) and thermal diffusivity (κ_d) values by $\kappa = d \times c_p \times \kappa_d$. The Seebeck coefficient was determined on an ULVAC ZEM-1 apparatus in He gas. The temperature gradients applied on the two ends of the pillar sample were 10–30 K. The estimated error for the Seebeck coefficient data was no more than 3%.

3. Results

3.1 Synthesis of the bulk $(Bi_{1-x}Sb_x)_2Te_3$ thermoelectric materials by MA-PDS

XRD patterns of the as-milled powders in Fig. 2 reveal a single $(Bi, Sb)_2Te_3$ phase in all the compositions. No remaining elemental powders or other compound phases were indexed. With increasing the antimony content the diffraction peaks shift to higher angles, indicating that alloying of the Sb atoms occurs during MA. The diffraction peak broadening was due to the grain size refinement and the introduction of atomic level strain. The above result confirmed that the substitutional solid solutions of $(Bi_{1-x}Sb_x)_2Te_3$ were formed over the entire compositional range of Sb under the current mechanical alloying conditions.

The mechanically alloyed powders were subsequently compacted into bulk by PDS. As shown in Fig. 3, all the compacts keep the single-phase state. And the $(Bi, Sb)_2Te_3$ crystals in the compacts have no obvious preferred crystallographic orientation. Table 1 lists the determined density and lattice parameters. Evidently, Sb alloying decreases the density of the compacts and the lattice parameters of the $(Bi, Sb)_2Te_3$ phase. For comparison, we prepared an ingot of $(Bi_{0.25}Sb_{0.75})_2Te_3$, where the calculated density is 6.77 g/cm^3, which is comparable to that (6.76 g/cm^3) of the sintered sample.

We employed SEM to observe the fracture surfaces of the compacts. In Fig. 4, one can see that all the compacts are dense and have very fine microstructures. The Sb content change makes little difference to the morphologies of the frac-

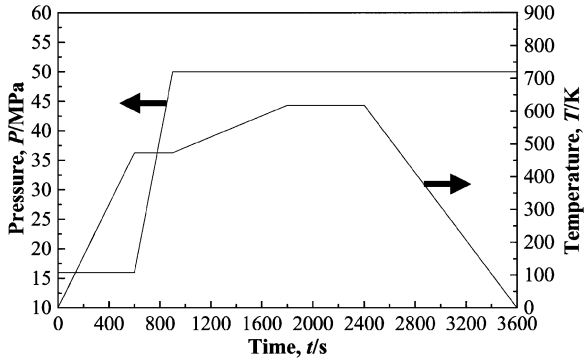

Fig. 1 Programs for temperature and pressure used in the pulse discharge sintering process.

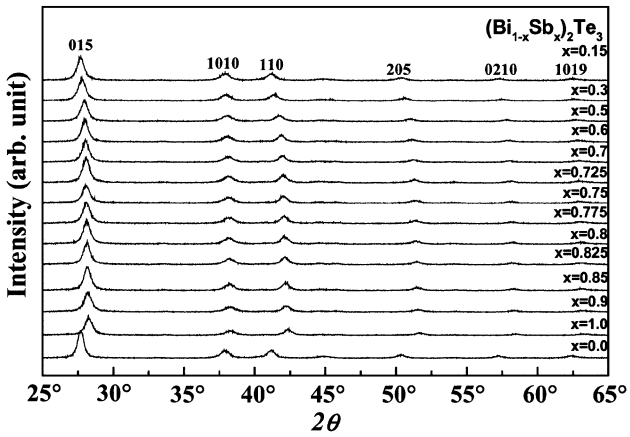

Fig. 2 XRD patterns of the mechanically alloyed powders.

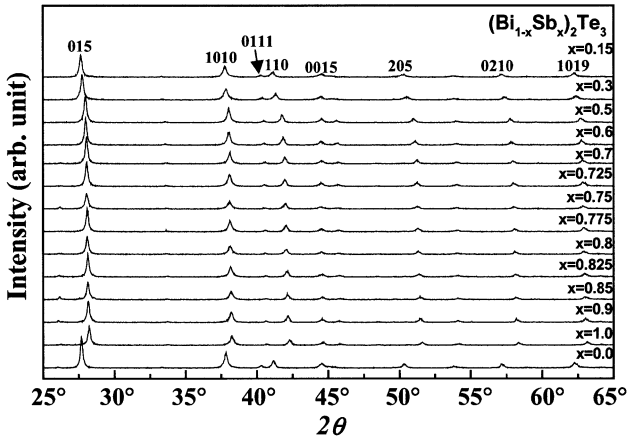

Fig. 3 XRD patterns of the sintered compacts.

Table 1 Density (d) of the compacts and lattice parameters of the $(Bi, Sb)_2Te_3$ phase in the compacts made by MA-PDS. The lattice parameters (a and c) were respectively calculated from the peak positions of (1019) and (205) lines.

x	d g/cm^3	a nm	c nm
0.0	7.67	0.438	3.051
0.15	7.44	0.438	3.050
0.3	7.22	0.436	3.049
0.5	7.08	0.432	3.048
0.6	6.82	0.431	3.048
0.7	6.79	0.430	3.047
0.725	6.78	0.429	3.047
0.75	6.76	0.430	3.047
0.775	6.72	0.429	3.046
0.8	6.67	0.429	3.043
0.825	6.65	0.429	3.043
0.85	6.63	0.428	3.043
0.9	6.61	0.428	3.043
1.0	6.44	0.427	3.042

ture surfaces. The average crystal size estimated from the cleavage plane is about several hundred nanometers.

3.2 Thermoelectric performance of the bulk $(Bi_{1-x}Sb_x)_2Te_3$ thermoelectric materials made by MA-PDS

The temperature dependence of Seebeck coefficient was illustrated in Fig. 5. Instead of a single sign of charge carriers, the type of the dominant charge carriers in the compacts shows strong Sb-content dependence. In the whole temperature range of 306–433 K, the samples with $x \leq 0.50$ display n-type semi-conducting and thus have a negative sign of Seebeck coefficient. At $x \geq 0.60$, however, the samples become p-type and have positive values of Seebeck coefficient. Higher values of Seebeck coefficient were achieved in region of $0.70 \leq x \leq 0.80$. At room temperature, the pure constituents of Bi_2Te_3 and Sb_2Te_3 as well as the n-type samples have comparatively low absolute values of Seebeck coefficient. In the p-type samples, the Seebeck coefficient increases with increasing x, reaches its maximum at $x = 0.725$ and then decreases.

The electrical resistivity of the sintered $(Bi_{1-x}Sb_x)_2Te_3$

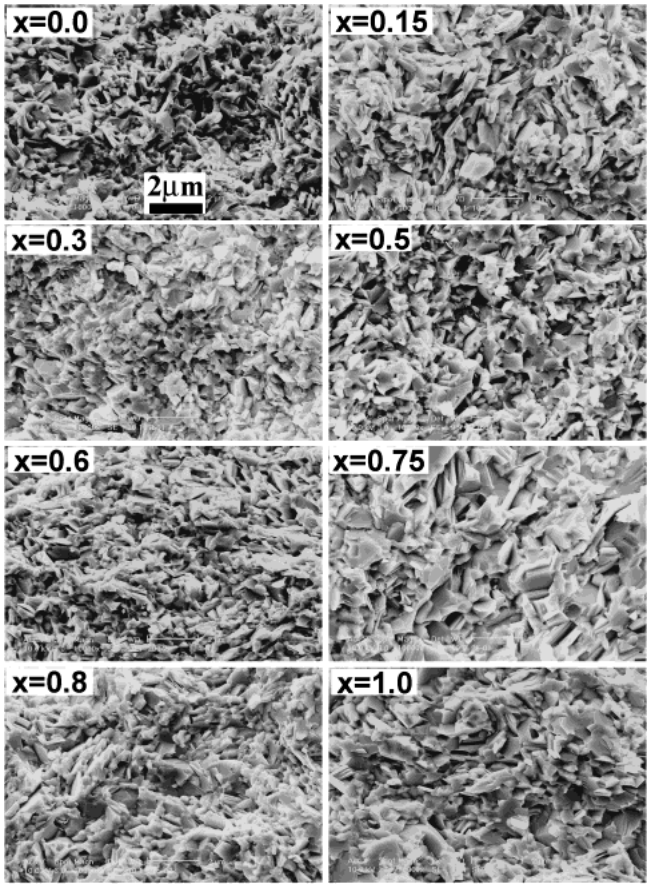

Fig. 4 SEM observations on the fracture surfaces of the $(Bi_{1-x}Sb_x)_2Te_3$ compacts.

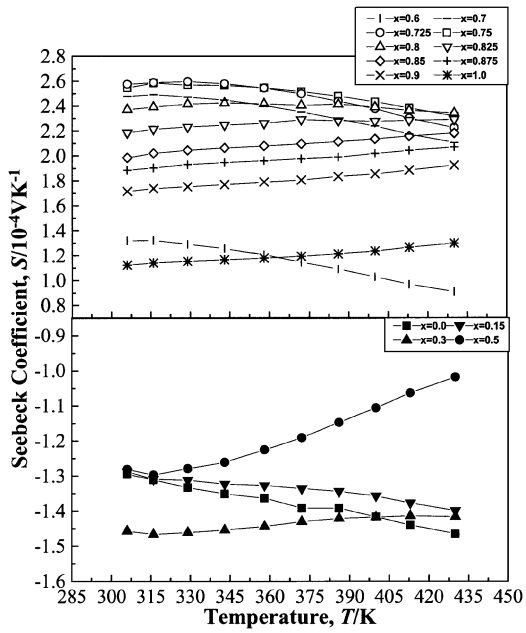

Fig. 5 Temperature dependence of Seebeck coefficient of the $(Bi_{1-x}Sb_x)_2Te_3$ compacts made by MA-PDS process.

samples was studied from 80 K to 380 K in Fig. 6. The weak temperature dependence of resistivity at low temperatures is characteristic of narrow band-gap nature of the current $(Bi, Sb)_2Te_3$ semiconductors. Interestingly, at $x = 0.30$, 0.50 and 0.60, the resistivity was found to decrease with temperature at above room temperature. In other words, intrin-

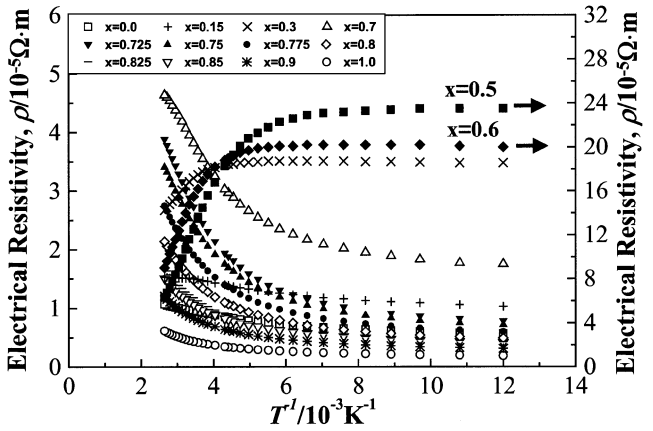

Fig. 6 Temperature dependence of electrical resistivity of the $(Bi_{1-x}Sb_x)_2Te_3$ compacts made by MA-PDS process.

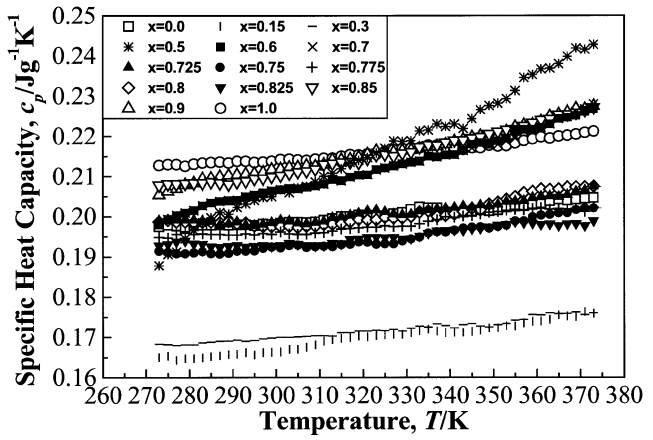

Fig. 7 Temperature dependence of specific heat capacity of the $(Bi_{1-x}Sb_x)_2Te_3$ compacts made by MA-PDS process.

sic conduction begins to predominate in these samples above room temperature. For other samples, however, the extrinsic conduction is predominant over the entire temperature range studied. It is noteworthy that the samples with $x = 0.50$ and 0.60 display much higher resistivity than other compositions. Based on these results, it is concluded that the Sb atoms strongly affect the electrical behaviors of the bulk samples.

The specific heat capacity (c_p) of the sintered compacts was determined from 273 K to 373 K by DSC. As seen in Fig. 7, c_p increases with temperature for all the compositions. The two n-type samples with $x = 0.15$ and 0.30 have much lower c_p values than other samples. The sample with $x = 0.50$ shows comparatively stronger temperature dependence of c_p than other compositions.

Table 2 summarizes all the experimental data used to calculate the room-temperature thermal conductivity. The pure Bi_2Te_3 and Sb_2Te_3 have fairly high values of thermal conductivity. Alloying of Sb is effective in reducing the magnitude of this parameter. The minimum value of 0.73 W/Km was achieved at $x = 0.60$, which is 55% smaller than that of the pure Bi_2Te_3.

Now, the room-temperature figure of merit can be estimated from the experimental Seebeck coefficient, electrical resistivity and thermal conductivity values. Table 3 lists all the experimental data for Z calculation. It is seen that the pure Bi_2Te_3 and Sb_2Te_3 as well as the samples with $x \leq 0.60$

Table 2 Room-temperature density (d), specific heat capacity (c_p), thermal diffusivity (κ_d) and total thermal conductivity (κ) of the bulk $(Bi_{1-x}Sb_x)_2Te_3$ samples made by MA-PDS.

x	d g/cm^3	c_p J/g·K	κ_d 10^{-2} cm^2/s	$\kappa (= d \cdot c_p \cdot \kappa_d)$ W/Km
0.0	7.67	0.198	1.061	1.61
0.15	7.44	0.177	0.925	1.22
0.3	7.22	0.170	0.605	0.74
0.5	7.08	0.206	0.643	0.94
0.6	6.82	0.206	0.522	0.73
0.7	6.79	0.208	0.563	0.80
0.725	6.78	0.193	0.642	0.84
0.75	6.76	0.192	0.700	0.91
0.775	6.72	0.196	0.657	0.86
0.8	6.67	0.197	0.701	0.92
0.825	6.65	0.199	0.744	0.98
0.85	6.63	0.210	0.793	1.10
0.9	6.61	0.212	0.897	1.26
1.0	6.44	0.214	1.574	2.17

exhibit Z values of the order of $1.0 \times 10^{-3}\,K^{-1}$. High Z values appear in the Sb-rich samples. The optimized figure of merit of $3.35 \times 10^{-3}\,K^{-1}$ was attained at $x = 0.80$. This composition corresponds to a comparatively higher $S^2\sigma$ and simultaneously a lower κ.

3.3 Hall effect of the bulk $(Bi_{1-x}Sb_x)_2Te_3$ thermoelectric materials made by MA-PDS

The Hall coefficients (R_H) of the sintered $(Bi_{1-x}Sb_x)_2Te_3$ samples were determined as a function of the reciprocal temperature in Fig. 8. It was found that both the magnitude and the sign of R_H were significantly affected by Sb. At low temperatures, R_H is almost constant. The pure Bi_2Te_3 as well as the two samples with $x = 0.15$ and 0.30 has negative Hall coefficients, meaning that these samples are n-type conducting in the temperature range studied. Interestingly, in the sample with $x = 0.50$ the measured R_H changes from positive to negative at around 300 K, which indicates that above 300 K the sample was changed from p-type to n-type. For the samples with $x \geq 0.60$, a p-type conduction is dominant from 80 to 380 K.

The carrier concentration was calculated from the Hall coefficient and was plotted as a function of reciprocal temperature in Fig. 9. One can see that the carrier concentration is quite sensitive to the Sb content. At low temperatures, the carrier concentration almost keeps constant in all the compositions. The pure constituents of Bi_2Te_3 and Sb_2Te_3 have the largest carrier concentration values. Alloying of Sb decreases the carrier density and the decrement strongly depends on x value. The n-type samples ($x = 0.0$, 0.15 and 0.30) have comparatively higher carrier densities than the p-type ternary solid solutions. With the increasing temperature, there is a jump in the carrier concentration of the sample with $x = 0.50$ at around 300 K. This can be reasonably ascribed to the p-n transition that took place at this temperature as confirmed by the change in the sign of Hall coefficient in Fig. 8. Obviously, among the samples we studied, $x = 0.50$ is the only case that shows a p-n transition in the Hall effect measurements.

Figure 10 presented the Hall mobility results of the

Table 3 Room-temperature transport properties of the bulk $(Bi_{1-x}Sb_x)_2Te_3$ samples made by MA-PDS.

x	S 10^{-4} V/K	σ $10^4(\Omega\cdot m)^{-1}$	$S^2\sigma$ 10^{-3} W/K^{2}m	κ W/Km	$Z(=S^2\sigma/\kappa)$ 10^{-3} K^{-1}	Carrier type
0.0	−1.30	10.34	1.75	1.61	1.09	n
0.15	−1.29	6.62	1.10	1.22	0.90	n
0.3	−1.46	3.16	0.67	0.74	0.91	n
0.5	−1.28	0.91	0.15	0.94	0.16	n
0.6	1.32	0.68	0.12	0.73	0.16	p
0.7	2.48	2.53	1.56	0.80	1.95	p
0.725	2.58	3.47	2.31	0.84	2.75	p
0.75	2.55	3.95	2.56	0.91	2.81	p
0.775	2.37	5.0	2.81	0.86	3.27	p
0.8	2.19	6.45	3.09	0.92	3.35	p
0.825	1.99	8.20	3.25	0.98	3.31	p
0.85	1.89	9.09	3.25	1.10	2.95	p
0.9	1.72	11.52	3.41	1.26	2.71	p
1.0	1.12	22.03	2.76	2.17	1.27	p

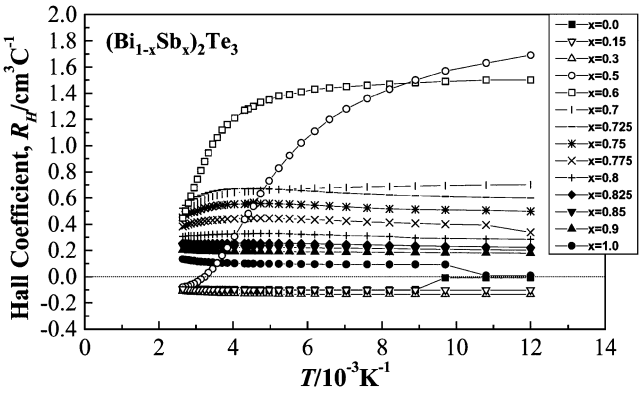

Fig. 8 Temperature dependence of Hall coefficient of the $(Bi_{1-x}Sb_x)_2Te_3$ compacts made by MA-PDS process.

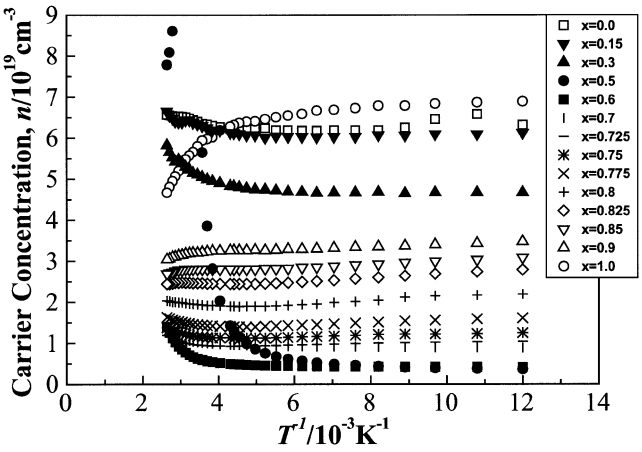

Fig. 9 Carrier concentration as a function of the reciprocal temperature of the $(Bi_{1-x}Sb_x)_2Te_3$ compacts made by MA-PDS process.

$(Bi_{1-x}Sb_x)_2Te_3$ samples. At low temperatures, all the n-type and the samples with $x = 0.50$ and 0.60 have small values of Hall mobility. The sample with $x = 0.725$ has the largest Hall mobility. With increasing temperature, the difference in Hall mobility data among samples is decreased.

A comparison of figure of merit and Hall parameters was made at room temperature in Table 4. All the n-type samples

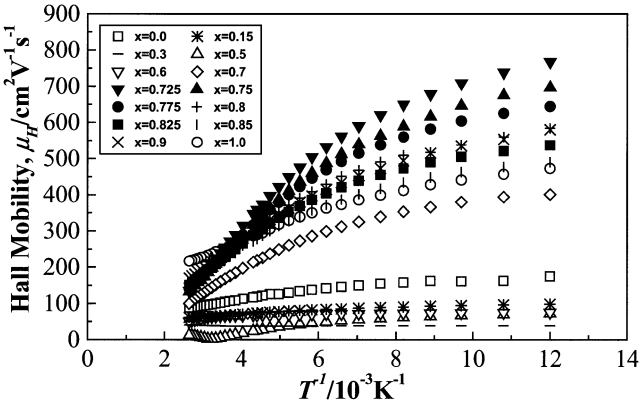

Fig. 10 Hall mobility as a function of the reciprocal temperature of the $(Bi_{1-x}Sb_x)_2Te_3$ compacts made by MA-PDS process.

have relatively high carrier concentration, low Hall mobility and small figure of merit values. At $x = 0.50$, the sample has the minimum values of Hall mobility and figure of merit. The optimum carrier density is 1.95×10^{19} cm^{-3}, which corresponds to the maximum Z of 3.35×10^{-3} K^{-1}.

4. Discussion

As described in the foregoing section, bismuth, tellurium and antimony form a continuous solid solution of $(Bi, Sb)_2Te_3$ by MA-PDS. All the bulk samples display the semi-conducting behavior within 80–380 K.

A comparison of room-temperature Seebeck coefficient of the $(Bi_{1-x}Sb_x)_2Te_3$ materials processed by different techniques was made in Fig. 11. It is noted that all the single crystals[4] are p-type semi-conducting, and the Seebeck coefficient shows a monotonic decrease with the Sb content. In the polycrystals, however, p-n transition occurs. The critical antimony content at which a p-n transition takes place is strongly dependent upon the sample preparation history. In the current MA-PDS cases, a p-n transition occurs at $x \approx 0.57$. In the case of mechanical grinding and hot press (MG-HP), Oh *et al.*[4] reported a p-n transition at $x \approx 0.67$, which is 10% higher than that of the current MA-PDS cases. For the thin

Table 4 Comparison of room-temperature figure of merit and Hall parameters of the bulk $(Bi_{1-x}Sb_x)_2Te_3$ samples made by MA-PDS.

x	Z 10^{-3} K^{-1}	R_H cm^3/C	n 10^{19} cm^{-3}	μ_H cm^2/Vs	Carrier type
0.0	1.09	−0.097	6.44	100	n
0.15	0.90	−0.098	6.38	65	n
0.3	0.91	−0.12	5.15	38	n
0.5	0.16	−0.0025	255	0.2	n
0.6	0.16	0.94	0.66	64	p
0.7	1.95	0.60	1.04	152	p
0.725	2.75	0.64	0.97	224	p
0.75	2.81	0.53	1.18	209	p
0.775	3.27	0.43	1.46	213	p
0.8	3.35	0.32	1.95	207	p
0.825	3.31	0.25	2.46	208	p
0.85	2.95	0.22	2.80	202	p
0.9	2.71	0.20	3.20	225	p
1.0	1.27	0.11	5.66	243	p

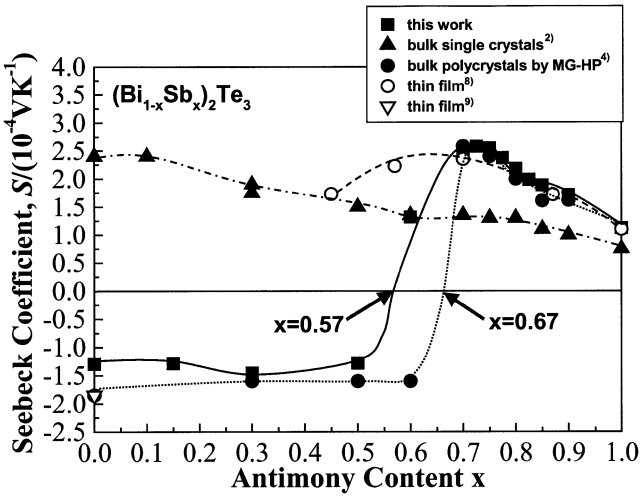

Fig. 11 Comparison of room-temperature Seebeck coefficient of the $(Bi_{1-x}Sb_x)_2Te_3$ samples synthesized by different techniques.

films prepared by CVD/PVD, the Seebeck coefficient data at lower Sb contents are unavailable in the literatures.[8,9] Nevertheless, one may expect that the p-n transition happens at much lower Sb content than in the sintered samples. As a result, the sample preparation history and the Sb content are two key factors determining the type of the dominant charge carriers in the $(Bi_{1-x}Sb_x)_2Te_3$ thermoelectric materials.

P-n transition is an interesting subject in the study of $(Bi, Sb)_2Te_3$ solid solutions. In the single crystals all the compositions show p-type at room temperature. It is suggested that Te atoms vaporize during melting process, leaving Te vacancies in the lattice. The anti-site defects are generated by occupation of Bi and Sb atoms into the vacant Te sites and simultaneously holes are produced. On the contrary, occupation of excess Te atoms in the Bi/Sb lattice sites will produce n-type carriers.[9,10] A previous study showed that in Bi_2Te_3 and Sb_2Te_3 crystals the concentration of the anti-site defects is in the order of 10^{19} cm^{-3}.[11] In the current MA-PDS process, mechanical alloying results in a high density of point defects and Te/Bi vacancies in the alloyed powders. It was reported[12] that more Te vacancies than Bi vacancies are generated during deformation of Bi_2Te_3-based alloys. These defects cannot be completely annealed out during the subsequent sintering process. It is believed that the remaining defects will exert considerable influence on the transport properties of the final product. In addition, oxygen contamination during powder handling also affects the p-n transition by adding donor levels.[13,14] Therefore, p-n transition is not controlled by only one mechanism. Detailed research on this subject is in progress.

The variations of Seebeck coefficient with temperature and Sb alloying levels are related to the change in the electronic structure near the Fermi energy. According to Boltzmann transport theory the Seebeck coefficient can be expressed as[15]

$$S = \frac{\pi^2 k_B^2 T}{3e} \frac{d(\ln \sigma(E))}{dE} \quad \text{at} \quad E = E_F, \tag{1}$$

where $\sigma(E)$ is the electrical conductivity determined as a function of energy, and E_F is the Fermi energy. Equation (1) suggests that S is optimized for the material that exhibits a rapid variation in $\sigma(E)$ within a few kT of the Fermi energy. Obviously, the unusual band structure, in particular, a steep band edge near the Fermi energy, is favorable for a high value of S. The complicated change in Seebeck coefficient with x value in Fig. 5 indicates the solid solution gives rise to complex band structures in the ternary Bi–Sb–Te system. At room temperature, the most favorable band structure is developed at $x = 0.725$, which corresponds to the maximum Seebeck coefficient. In the presence of the detailed data on the band structure, it is difficult to suggest a quantitative explanation of the experimental results in Fig. 5.

On the other hand, the Seebeck coefficient of the p-type TE materials in the extrinsic conduction region can be expressed as[16]

$$S = k_B[\gamma + C - \ln(n)]/e. \tag{2}$$

Here k_B is the Boltzmann constant, γ the scattering related factor ($\gamma = 0$ for lattice scattering and 2 for impurity scattering), C the constant and n the carrier concentration. Based on the above equation, the decreased Seebeck coefficient at $x > 0.725$ can be reasonably attributed to the increased number of carriers, as shown in Table 4.

As is well-known that the electrical conductivity (σ) is proportional to the carrier concentration (n) and carrier mobility (μ) by $\sigma = ne\mu$, we can qualitatively understand the electrical behaviors of the sintered $(Bi_{1-x}Sb_x)_2Te_3$ samples in Fig. 6 from the carrier concentration and Hall mobility results in Figs. 8 and 9. At low temperatures, it is evident that the extremely low carrier mobility is responsible for the large resistivity of the samples with $x = 0.50$ and 0.60. The good electrical conductivity of the pure constituents of Bi_2Te_3 and Sb_2Te_3 is closely related to the high carrier concentrations in them. Alloying of Sb decreases, more or less, the carrier concentration, but exerts a complicated influence on the Hall mobility. With increasing temperature, a p-n transition occurs at around room temperature in the sample with $x = 0.50$, which is characterized by a rapid increase in the carrier density with temperature. Note that the intrinsic conduction takes place in the samples with $x = 0.30$, 0.50 and 0.60 above room temperature.

Quantitative determinations of lattice parameters of the

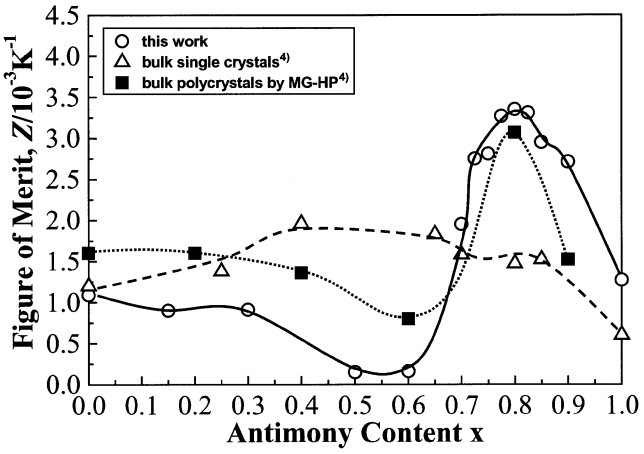

Fig. 12 Comparison of room-temperature figure of merit of the bulk $(Bi_{1-x}Sb_x)_2Te_3$ samples prepared by three different techniques.

$(Bi, Sb)_2Te_3$ phase in Table 1 indicate that the unit cell of the $(Bi, Sb)_2Te_3$ phase shrinks as more Sb atoms are alloyed because of the relatively small size of the antimony atoms. The lattice disordering caused by Sb alloying acts as effective scattering on phonons, leading to a decreased lattice thermal conductivity.[17] The compositional dependence of thermal conductivity in Table 2 shows that the most effective scattering is realized at $x = 0.60$.

We compared the room-temperature figure of merit of the bulk $(Bi_{1-x}Sb_x)_2Te_3$ materials produced by different techniques in Fig. 12. For single crystals,[4] the obtained Z values vary within 1.0–2.0 $\times 10^{-3}\,K^{-1}$. Enhanced Z values that are close to or greater than $3 \times 10^{-3}\,K^{-1}$ are available in the sintered polycrystals in the Sb-rich side. Irrespective of the processing techniques, the optimized Z values appear at $x = 0.80$ for the sintered polycrystals. At $x = 0.80$, the sample made by MA-PDS shows a figure of merit of $3.35 \times 10^{-3}\,K^{-1}$, which is higher than that ($3.07 \times 10^{-3}\,K^{-1}$) of the sample by MG-HP.[4] The decreased thermal conductivity is an important consideration for the enhancement in Z. In this way, the current MA-PDS approach is highlighted in that it is simple in processing and the Sb-rich, p-type products display high values of figure of merit at room temperature, say, $3.35 \times 10^{-3}\,K^{-1}$ at $x = 0.80$.

5. Conclusions

In this study, high-quality $(Bi_{1-x}Sb_x)_2Te_3$ bulk thermoelectric materials that are dense and have refined microstructures have been successfully fabricated by means of a new processing technique, namely mechanical alloying followed by pulse discharge sintering (MA-PDS). Systematic transport property measurements demonstrate that the electrical, thermal and thermoelectric properties of the sintered $(Bi_{1-x}Sb_x)_2Te_3$ compacts are quite sensitive to the Sb content. At room temperature, the samples show n-type semi-conducting at $x < 0.57$. At $x > 0.57$, however, the samples become p-type. A p-n transition happens in the sample with $x = 0.50$ at around room temperature. For other compositions, a single sign of charge carrier is predominant and therefore no p-n transition is detectable within 80–433 K. High values of room-temperature figure of merit are realized in the Sb-rich, p-type samples. The maximum value of $3.35 \times 10^{-3}\,K^{-1}$ is attained at $x = 0.80$, which corresponds to the carrier concentration and Hall mobility of $1.95 \times 10^{19}\,cm^{-3}$ and $207\,cm^2/Vs$, respectively. The current MA-PDS processing is highlighted in efficiently producing the bulk, Sb-rich $(Bi, Sb)_2Te_3$ thermoelectric materials that exhibit enhanced room-temperature figure of merit.

Acknowledgements

One of the authors (LXD) is grateful to the STA Fellowship during his research in Japan. Valuable suggestion and comments from referees are greatly appreciated.

REFERENCES

1) M. Stordeur and H. Sobotta: *Proc. First European Conf. on Thermoelectrics*, ed. by D. M. Rowe (Peregrinus Ltd., London, 1988) pp. 209–212.
2) H. Scherrer and S. Scherrer: *CRC Handbook of Thermoelectrics*, ed. by D. M. Rowe (CRC Press, Inc., 1995) pp. 211–255.
3) C. Wood: Energy Convers. Mgmt. **24** (1984) 317–322.
4) T. S. Oh, D. B. Hyun and N. V. Kolomoets: Scr. Mater. **42** (2000) 849–854.
5) J. Yang, T. Aizawa, A. Yamamoto and T. Ohta: J. Alloys Comp. **309** (2000) 225–228.
6) H. C. Kim, T. S. Oh and D. B. Hyun: J. Phys. Chem. Solids **61** (2000) 743–747.
7) X. D. Liu and Y. H. Park: Mater. Trans. **43** (2002) 30–35.
8) A. Giani, A. Boulouz, F. Pascal-Delannoy, A. Foucaran and A. Boyer: Thin Solid Films **315** (1998) 99–103.
9) S. Cho, Y. Kim, A. Divenere, G. K. Wong and J. B. Ketterson: J. Appl. Phys. **75** (1999) 1401–1404.
10) T. C. Harman, S. E. Miller and H. L. Goeing: Bull. Am. Phys. Soc. **30** (1955) 35–41.
11) J. Horak, L. Tichy, P. Lostak and A. Vasko: Cryst. Lattice Defects **6** (1976) 223–228.
12) J. M. Schultz, J. P. McHugh and W. A. Tiller: J. Appl. Phys. **33** (1962) 2443–2447.
13) D. M. Gel'fgat and Z. M. Dashevskii: Inorg. Mater. **19** (1984) 1172–1175.
14) B. Y. Jung, T. S. Oh, D. B. Hyun and J. D. Shim: J. Kor. Phys. Soc. **31** (1997) 219–223.
15) R. D. Barnard: *Thermoelectricity in Metals and Alloys*, (Taylor & Francis, London, 1972) pp. 102–112.
16) J. Seo, K. Park, D. Lee and C. Lee: Scr. Mater. **38** (1998) 477–481.
17) M. Stordeur: *CRC Handbook of Thermoelectrics*, ed. D. M. Rowe (CRC Press, Inc., 1995) pp. 239–255.